Electronic Supplementary Material (ESI) for ChemComm.
This journal is © The Royal Society of Chemistry 2023

Supporting Information

Homogeneous voltammetric sensing strategy of lead ion based on aptamer gated methylthionine chloride@UiO-66-NH_2 framework as smart target-stimulated responsive nanomaterial

Tingting Liu,[a] Ruiyong Zhou,[a] Conglin Zhang,[a] Yinhui Yi,[a] Gangbing Zhu [a,b*]

[a] School of the Environment and Safety Engineering, Collaborative Innovation Center of Technology and Material of Water Treatment, Jiangsu University, Zhenjiang, 212013, P. R. China

[b] Department of Applied Biology and Chemical Technology, and the State Key Laboratory of Chirosciences, The Hong Kong Polytechnic University, Hung Hom, Kowloon Hong Kong

*Corresponding author. E-mail address: zhgb1030@ujs.edu.cn. Tel.: +86 511 88791800; fax.: +86 511 88791800.

EXPERIMENTAL SECTION

Reagents and Instruments

1-ethyl-3-(3-dimethylaminopropyl) carbodiimide (EDC), N-hydroxy succinimide (NHS) and Me were obtained from Macklin Biochemical Technology Co., Ltd. (China). N, N-dimethylformamide (DMF), methanol, $ZrCl_4$, 2-amino terephthalic acid (NH_2-H_2BDC), HNO_3, CH_3COOH and Tris (hydroxymethyl) aminomethane (Tris) were achieved from Aladdin Reagent Co., Ltd. (Shanghai, China). KCl, NaCl, AgCl, $MgCl_2$, $MnCl_2$, $CaCl_2$, $CdCl_2$, $CuCl_2$, $FeCl_2$, $HgNO_3$, $ZnCl_2$, $CoCl_2$, $Pb(NO_3)_2$ and $FeCl_3$ were purchased from Sinopharm Chemical Reagent Co., Ltd. (China). Ultrapure water (UPW) was obtained via Milli-Q ultrapure water purification system (Millipore).

The used Apt and CP were provided by Shanghai Sangon Biotechnology Co., Ltd. (China). and the sequences were as follows:

Apt: 5′-GGTTGGTGTGGTTGG-3′.

CP: 5′-COOH-TAG TTT AGC CCA ACC ACA CCA ACC-3′.

The specific instruments were listed as follows:

Scanning electron microscope (SEM, JSM-7800F, Japan); Transmission electron microscopy (TEM; JEM-2100, Japan); X-ray diffraction (XRD, Bruker D8 ADVANCE, Germany); Raman spectrometer (DXR, Thermo Fisher, USA); X-ray photoelectron spectrometer (XPS, AXIS-Ultra DLD, Japan); Fourier transform infrared spectroscopy (FT-IR, Nicolet Thermo, USA). Energy dispersive spectroscopy (EDS) elemental mapping images and spectrum analysis were conducted using a JEM-1400 Plus field-emission TEM. The Zeta potentials were measured on Malvern Nano-ZS Zeta Sizer (Malvern, UK). All the electrochemical tests were performed on the CHI660E electrochemical workstation with a three-electrode cell: The glassy carbon electrode (GCE) and saturated calomel electrode, platinum wire were served as the working, reference and auxiliary

electrode, respectively. Brunauer-Emmett-Teller (BET, JW-BK2008, China) analysis was used to examined the specific surface area, the pore volume and pore diameter of UiO-66-(NH_2) at 77.35K.

Preparation of UiO-66-NH_2

The UiO-66-NH_2 MOF structure was prepared by one-pot hydrothermal synthesis method according to the previous reports with some modifications.[1, 2] $ZrCl_4$ (46.7 mg) and NH_2-H_2BDC (36.3 mg) were dissolved in 20.42 mL DMF solution containing 4.58 mL acetic acid (17.5 M). The mixture was sonicated for 10 minutes and then transferred to 50 mL Teflon reactor. The container was capped and placed at 120 ℃ for 12 h to yield UiO-66-NH_2. The precipitate was washed with methanol/DMF three times, then dried overnight in a vacuum at 60 °C.

Construction of Me@UiO-66-NH_2

Before constructing Me@UiO-66-NH_2, CP solution was first loaded onto UiO-66-NH_2 (CP-UiO-66-NH_2). Firstly, 500 μL CP solution (10.0 μM), 250 μL EDC (5.0 mg mL^{-1}), and 250 μL NHS (5.0 mg mL^{-1}) were mixed to form a homogeneous solution and incubated for 30 minutes to activate the -COOH groups of CP. Subsequently, 10.0 mg UiO-66-NH_2 was added, and CP-terminated MOF material (CP-UiO-66-NH_2) was successfully prepared after the mixture system stirring at room temperature for 15 h. The reaction solution was washed through centrifugation and redispersed in UPW of 1.0 mL for subsequent use. For preparing Me@UiO-66-NH_2, 100 μL CP-UiO-66-NH_2 solution and 100 μL Me solution were added to 800 μL UPW and stirred for 12 h at room temperature. Next, to encapsulate Me into UiO-66-NH_2, 100 μL Apt solution (1.0 mM) was added to the above mixture and incubated for 3 h to form Me@UiO-66-NH_2. Eventually, the suspension was washed three times with UPW and dispersed in 1.0 mL UPW for future use.

Electrochemical sensing of Pb^{2+}

For the HVC detection of Pb^{2+}, 40 μL of Me@UiO-66-NH_2, and 200 μL target Pb^{2+} sample with

different concentrations were incubated together. After that, the 760 μL Tris-HAC buffer (0.01 M, pH=7.4) was added into the reaction system and the electrochemical sensing was performed by using differential pulse voltammetry (DPV) in the potential range from -0.50 V to -0.10 V.

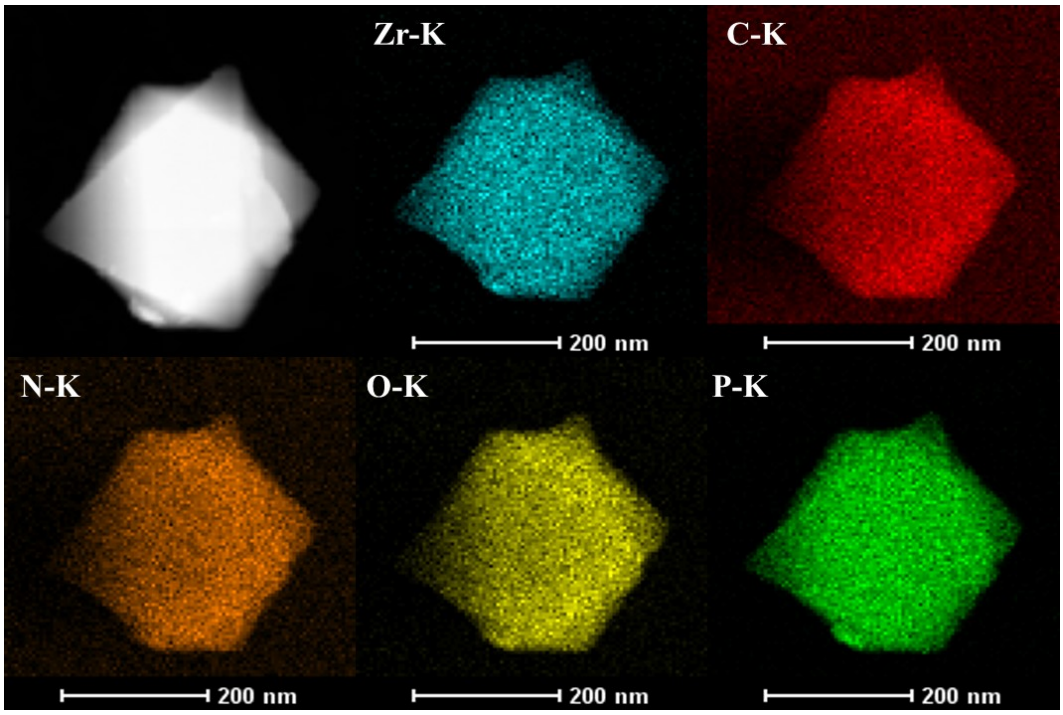

Figure S1. HRTEM image of the prepared Me@UiO-66-NH_2 and the corresponding EDS elemental mappings of Zr, C, N, O, and P elements.

The typical energy dispersive spectroscopy (EDS) mapping image of Me@UiO-66-NH_2 was performed, the results show that there are five elements (Zr, C, N, O and P) presented and distributed equally in Me@UiO-66-NH_2 (Figure S1).

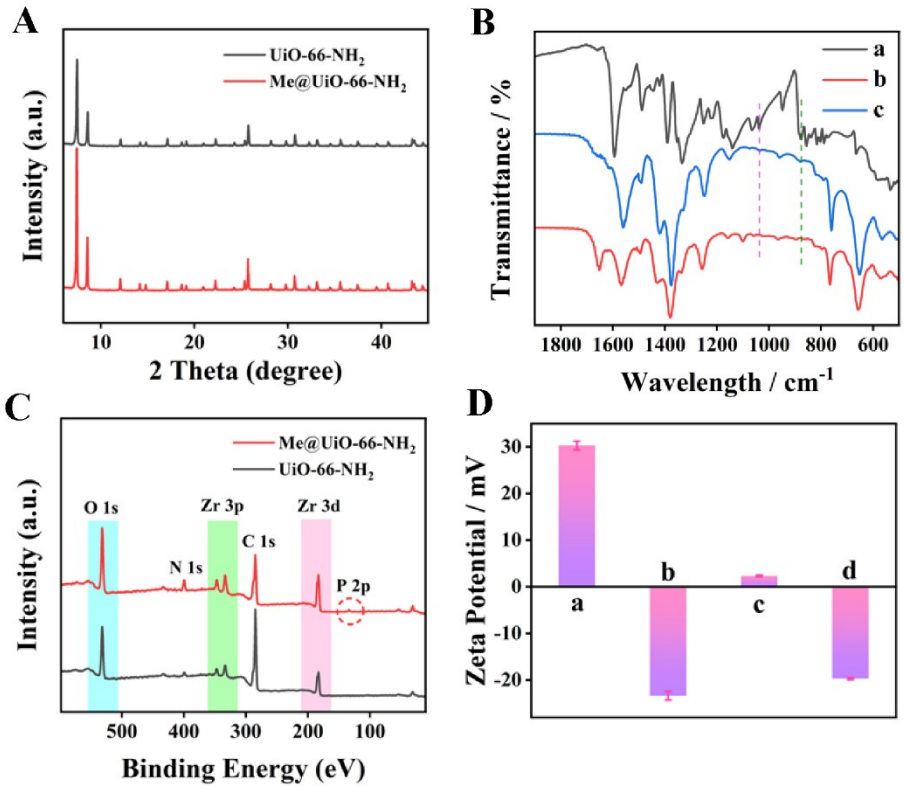

Figure S2. (A) XRD analysis of UiO-66-NH_2, and Me@UiO-66-NH_2; (B) FT-IR spectra of Me (a), UiO-66-NH_2 (b), and Me@UiO-66-NH_2 (c); (C) XPS spectra of UiO-66-NH_2, and Me@UiO-66-NH_2; (D) Zeta potential values of UiO-66-NH_2 (a), CP (b), CP-UiO-66-NH_2 (c) and Me@UiO-66-NH_2 (d).

The XRD test was performed to indicate the crystalline pattern and phase purity. As depicted in Figure S2A, the prepared Me@UiO-66-NH_2 (red line) was consistent with UiO-66-NH_2 (black line), which further suggested that the Me encapsulation had basically no effect on the lattice structure of UiO-66-NH_2. Meanwhile, there is no characteristic peak of Me molecule found, indicating that the Me probe was encapsulated successfully in the UiO-66-NH_2 framework rather than on its surface. Figure S2B displayed the FT-IR spectrums of UiO-66-NH_2 and Me@UiO-66-NH_2, the results showed that the spectra of both are basically identical, and the new absorbing bands resulted from

Me at 1135 cm^{-1} and 883 cm^{-1} are presented for Me@UiO-66-NH_2,[3] which also proves that Me was successfully encapsulated into the UiO-66-NH_2 structure.

To study the elemental composition and valence states of the Me@UiO-66-NH_2 smart material, the XPS analysis was carried out and the corresponding results were shown in Figure S2C. It can be clearly observed that the XPS curves of both UiO-66-NH_2 and Me@UiO-66-NH_2 were almost the same, and they exhibit four distinct peaks at 284.8, 399.8, 531.8 and 182.8 eV corresponding respectively to C 1s, N 1s, O 1s and Zr 3d. In addition, as for Me@UiO-66-NH_2, there was a peak observed at 133.7 eV, which is corresponding to P element, proving that the Apt was successfully capped on the UiO-66-NH_2 framework. Meanwhile, the Zr 3d peaks can be deconvoluted into two constituents: $3d_{5/2}$ peak (182.82 eV) and $3d_{3/2}$ peak (185.20 eV) (Figure S3). Furthermore, the Zeta potential was measured to investigate the electrophoretic mobility and proved the surface functionalization of the MOF materials. As displayed in Figure S2D, it can be noted that the Zeta potentials of the prepared UiO-66-NH_2 (a), CP (b), CP-UiO-66-NH_2 (c) and Me@UiO-66-NH_2 (d) were +30.3 mV, -23.4 mV, +2.32 mV and -19.7 mV, respectively. The UiO-66-NH_2 showed electro-positivity and the CP exhibited electronegativity. Compared to the zeta potential from UiO-66-NH_2, the potential of CP-UiO-66-NH_2 showed a significant change, whereas it still remained positive due to the positive properties of the Me.[4] As the Apt was stepped on, the potential of the composite decreased dramatically. This change of zeta potentials indirectly proved the Apt was successfully modified on the UiO-66-NH_2.

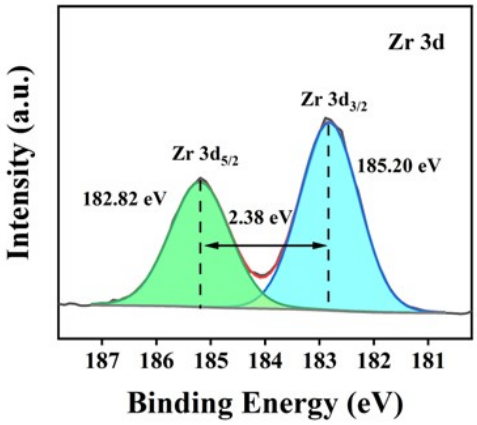

Figure S3. XPS spectra of Zr 3d spectra of Me@UiO-66-NH_2.

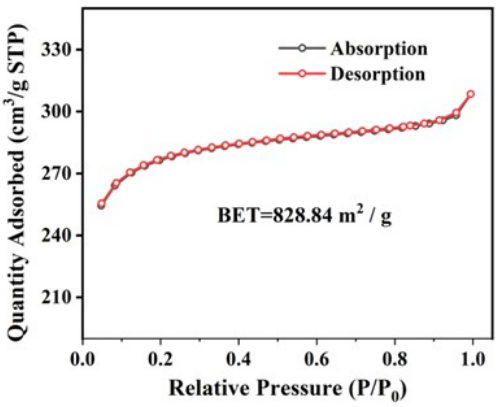

Figure S4. N_2-absorption-desorption isotherm and

The surface area, pore size, and pore volume of the obtained UiO-66-NH_2 were evaluated by the BET analysis and the related N_2 adsorption-desorption isotherm was shown in Figure S4. It can be calculated that the BET surface area and pore volume of UiO-66-NH_2 are 828.84 m^2 g^{-1} and 0.349 cm^3 g^{-1}, respectively. These results demonstrated that the as-prepared UiO-66-NH_2 can exhibit large specific surface area, typical microporous characteristics and high adsorption performance,[5, 6] which provided suitable conditions for Me entering and encapsulated in the inside of UiO-66-NH_2.

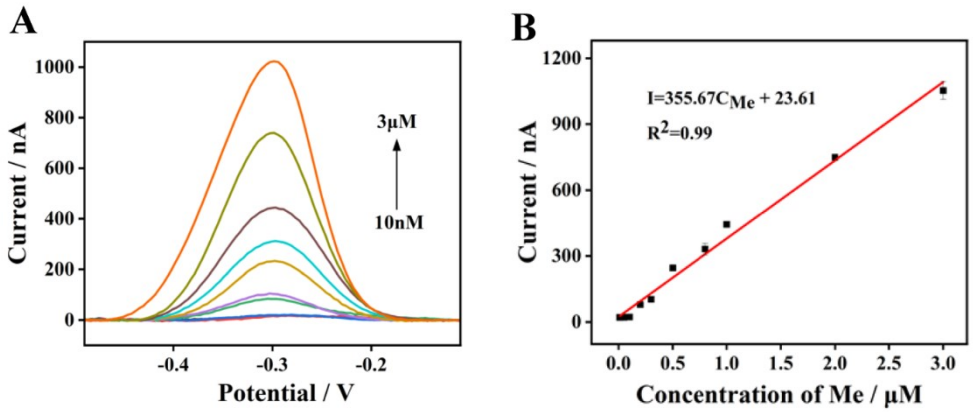

Figure S5. (A) DPV responses of Me at different concentrations; (B) Linear relationship between the current and the concentration of Me.

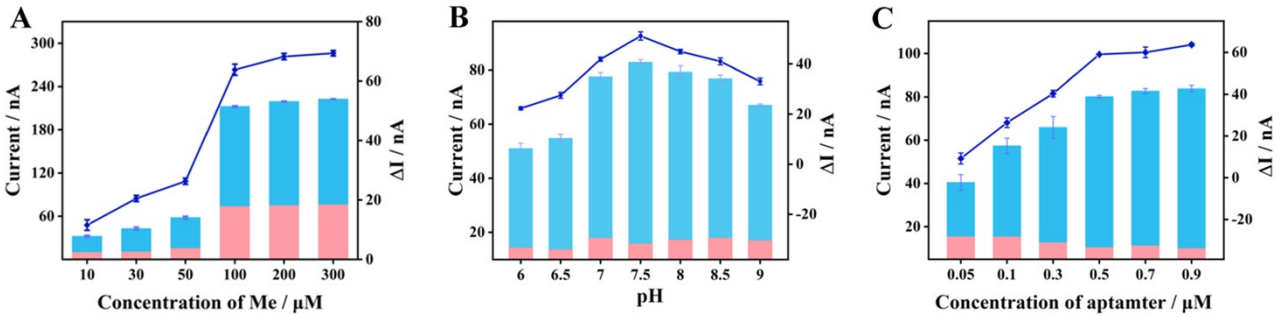

Figure S6. Optimization of the experimental parameters for the detection of Pb^{2+}: (A) the concentration of Me, (B) the pH value and (C) the concentration of aptamer.

In order to achieve the best detection performance, several key experimental conditions were optimized and the related results were exhibited in Figure S6, which includes the effect from (A) the concentration of Me, (B) the pH value and (C) the concentrations of Apt, where ΔI is the DPV current change of the sensing system in the absence and presence of Pb^{2+}. It can be seen from the Figure S6A that the current signals and ΔI values increased with the increase of the Me concentration from 10.0 to 100.0 μM, which indicated that more Me is encapsulated into the UiO-66-NH_2 framework. But when the concentration exceeds 100.0 μM, the current becomes almost stable, so the optimal concentration of Me was chosen as 100.0 μM. In addition, the pH value of detection system is also an important factor. As revealed in Figure S6B, the signal responses increased with the increase of pH value in the range of 6.0-7.5, and when the pH value exceeds 7.5, the signal responses decrease obviously. The reason is that the structure and performance of Apt will be greatly affected at excessively acidic or alkaline conditions,[7] thus 7.5 was chosen as the optimum pH value. Furthermore, as an important parameter acting as a guarder, it is necessary to study the concentration of Apt. Figure S6C shows that the ΔI values gradually increase with the increase of the Apt concentration and reaches a maximum when the concentration increases to 0.5 μM. Therefore, the 0.5 μM was selected as the optimal concentration of Apt.

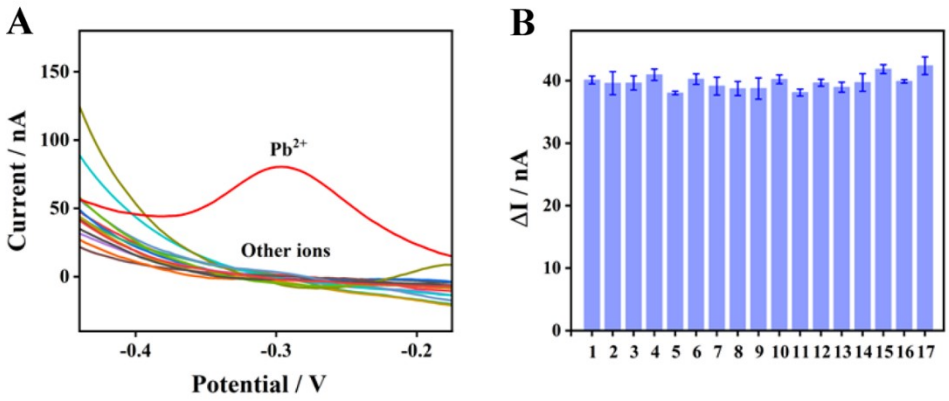

Figure S7. (A) DPV responses of the as-developed HVC sensor towards various interfering ions (Na^+, K^+, Ag^+, NH_4^+, Mg^{2+}, Mg^{2+}, Mn^{2+}, Ca^{2+}, Cd^{2+}, Cu^{2+}, Fe^{2+}, Hg^{2+}, Zn^{2+}, Co^{2+}, Ni^{2+}, and Fe^{3+}). (B) anti-interference experiment of the HVC sensor via adding various interfering ions to Pb^{2+} solution: (1) Na^+, (2) K^+, (3) Ag^+, (4) NH_4^+, (5) Mg^{2+}, (6) Mn^{2+}, (7) Ca^{2+}, (8) Cd^{2+}, (9) Cu^{2+}, (10) Fe^{2+}, (11) Hg^{2+}, (12) Zn^{2+}, (13) Co^{2+}, (14) Ni^{2+}, (15) Pb^{2+}, (16) Fe^{3+}, (17) Mixture.

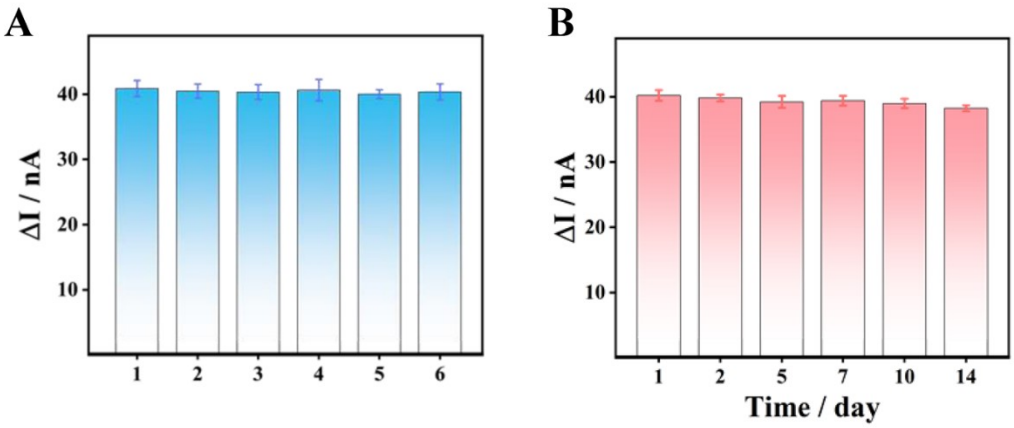

Figure S8. (A) DPV current obtained from six independently prepared Me@UiO-66-NH_2 sensing platforms to detect the Pb^{2+}. (B) Stability investigation of Me@UiO-66-NH_2 for different storage times.

In order to study the repeatability of the proposed sensor, we prepared six independent sensing platforms to carry out the same experimental procedures. The experimental results showed that the relative standard deviation value is less than 2.47% (Figure S8A), suggesting that the designed Me@UiO-66-NH_2-based HVC sensing sensor has excellent reproducibility. In addition, for studying the stability of the as-prepared Me@UiO-66-NH_2, the electrochemical response of the HVC sensor to Pb^{2+} was tested after storing the material in refrigerator for 15 days. The results showed that the current signal decreased only by 1.9% compared with the initial current response (Figure S8B), indicating an acceptable stability of the proposed HVC sensor. In addition, after reacting with Pb^{2+} for 60 min, the Me@UiO-66-NH_2 framework remained unchanged (Figure S9), identifying that the addition of Pb^{2+} did not lead to the collapse of the organic skeleton, which still maintained a stable frame structure. In conclusion, the designed HVC sensor offers good repeatability and stability for Pb^{2+} detection.

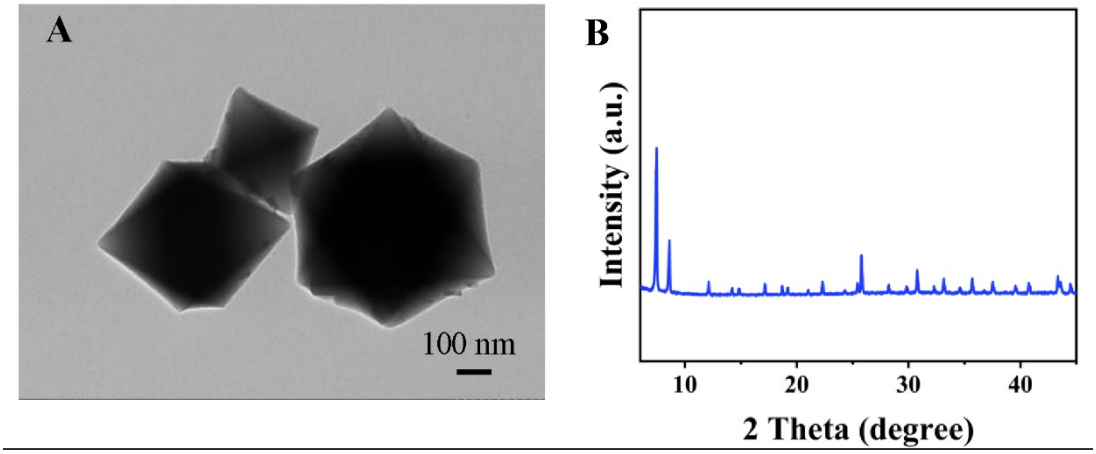

Figure S9. (A) TEM image of Me@UiO-66-NH_2 after reacting with Pb^{2+}. (B) XRD of Me@UiO-66-NH_2 after reacting with Pb^{2+}.

After the treatment with Pb^{2+} for 60 min, the TEM image shows the Me@UiO-66-NH_2 framework remains unchanged. Furthermore, the XRD pattern of Me@UiO-66-NH_2 after reacting with Pb^{2+} coincided with that of pure Me@UiO-66-NH_2, verifying that the crystal structure of Me@UiO-66-NH_2 was not destroyed after adding Pb^{2+}.

Table S1. Comparison of the designed HVC sensor with the previous methods for Pb^{2+}.

Method	Linearity (M)	LOD (M)	Remark		Reference
			Electrode modification	Electrodeposition	
Fluorescence	2.0×10^{-8} - 1.0×10^{-4}	6.5×10^{-10}			8
Fluorescence	1.0×10^{-10} - 1.0×10^{-8}	9.0×10^{-11}			9
Fluorescence	5.0×10^{-7} - 4.0×10^{-5}	5.0×10^{-7}			10
Colorimetric	1.0×10^{-4} - 4.0×10^{-3}	1.8×10^{-6}			11
Colorimetric	/	3.0×10^{-7}			12
Colorimetric	5.0×10^{-9} - 2.0×10^{-6}	1.6×10^{-9}			8
Colorimetric	2.0×10^{-6} - 2.5×10^{-5}	2.0×10^{-6}			13
EC sensor	9.9×10^{-14} - 9.9×10^{-13}	3.3×10^{-15}			14
EC aptasensor	5.0×10^{-12} - 1.0×10^{-6}	1.7×10^{-12}			15
PEC aptasensor	5.0×10^{-12} - 1.0×10^{-8}	1.6×10^{-12}			16
ECL aptasensor	1.0×10^{-15} - 1.0×10^{-8}	1.9×10^{-16}			7
Electrochemistry	1.0×10^{-10} - 1.0×10^{-6}	1.6×10^{-11}	Au/CP/MCH/Apt, 17.5 h		17
Electrochemistry	1.0×10^{-12} - 2.0×10^{-9}	9.8×10^{-12}	MCH /HBA/PBA /AuE, 11.25 h		18
Electrochemistry	5.0×10^{-11} - 5.0×10^{-6}	5.0×10^{-12}	Au/DNA2, 8 h		19
Electrochemistry	5.0×10^{-9} - 5.0×10^{-6}	1.7×10^{-12}	Cu-TCPP/Au/Pb^{2+}-G4-hemin, 5.5 h		20
Electrochemistry	4.8×10^{-9} – 4.8×10^{-3}	1.4×10^{-10}	PolyA assembly AuE, 24 h		21
Electrochemistry	4.8×10^{-12} – 4.8×10^{-9}	1.59×10^{-12}	CS/RGO/TiO_2, 13.5 h		22
Electrochemistry	1.0×10^{-11} - 1.0×10^{-6}	8.7×10^{-12}	2D MOF, 4 h		23
Electrochemistry	5.0×10^{-7} - 3.0×10^{-6}	1.11×10^{-9}	ZIF-67	−1.0 V, 400 s	24
Electrochemistry	1.78×10^{-8} - 1.78×10^{-6}	4.1×10^{-8}	GODs-NF	−1.3 V, 150 s	17
Electrochemistry	1.9×10^{-7}- 4.8×10^{-6}	7.4×10^{-8}	poly PCA/GE	− 1.6 V, 125 s	25
Electrochemistry	4.8×10^{-9} - 1.4×10^{-6}	8.2×10^{-10}	RGO-S/PGE	− 1.2 V, 270 s	26
Electrochemistry	1.9×10^{-12} – 5.8×10^{-10}	6.3×10^{-13}	GO-Fe_3O_4-PAMAM	− 1.1 V, 160 s	27
Electrochemistry	1.9×10^{-12} – 2.4×10^{-10}	2.4×10^{-12}	PVA/chitosan-TRG	− 0.9 V, 300 s	28
Electrochemistry	1.0×10^{-9} - 1.0×10^{-6}	1.72×10^{-9}	GDY	− 1.2 V, 600 s	29
Electrochemistry	5.0×10^{-13} - 5.0×10^{-7}	1.66×10^{-13}	Free		This work

Table S2. Recovery and RSD of the designed HVC sensor for Pb^{2+} detection in real samples. (n=3)

Samples	Spiked (nM)	Found (nM)	Recovery (%)	RSD (%)
Tap water	0.10	0.1047	104.70	4.74
	1.00	1.061	106.10	3.72
	100.00	101.72	101.72	2.14
Lake water	0.10	0.1072	107.20	4.09
	1.00	0.977	97.70	2.51
	100.00	102.30	102.30	1.86

To assess the validity of the proposed HVC sensor in practical application, it was carried out to detect Pb^{2+} in real sampled including tap water and lake water via the standard addition method, and the corresponding results were shown in Table S2. It can be observed from the table that the recoveries ranged from 97.70% to 107.20%, and the relative standard deviation (RSD) is lower than 4.74%. Based on these results, it can be confirmed that the as-proposed HVC sensor has satisfactory accuracy and reliability, which suggested a significant potential for the practical samples.

References:

1. D. Wang, S. Li, C. Wu, T. Li, *Journal of the American Chemical Society*, 2022, **144**, 685-689.
2. S. Li, B. He, Y. Liang, J. Wang, Q. Jiao, Y. Liu, R. Guo, M. Wei, H. Jin, *Analytica chimica acta*, 2021, **1182**, 338948.
3. J. Chang, W. Lv, Q. Li, H. Li, F. Li, *Analytical Chemistry*, 2020, **92**, 8959-8964.
4. J. Feng, C. Chu, K. Dang, T. Yao, Z. Ma, H. Han, *Analytica chimica acta* , 2021, **1187**, 339170.
5. N. Zhang, D. Li, M. Mu, M. Lu, *Chemical Engineering Journal*, 2022, **448**, 137467.
6. Y. Cai, H. Zhu, W. Zhou, Z. Qiu, C. Chen, A. Qileng, K. Li, Y. Liu, *Analytical Chemistry*, 2021, **93**, 7275-7282.
7. X. Liu, L. Li, F. Li, W. Zhao, L. Luo, X. Bi, X. Li, T. You, *J Hazard Mater*, 2022, **424**, 127480.
8. J. Xu, Y. Zhang, L. Li, Q. Kong, L. Zhang, S. Ge, J. Yu, *ACS Applied Materials & Interfaces*, 2018, **10**, 3431-3440.
9. M. Li, X. Zhou, S. Guo, N. Wu, *Biosensors and Bioelectronics*, 2013, **43**, 69-74.
10. C.-J. Liu, J. Ling, X.-Q. Zhang, J. Peng, Q.-E. Cao, Z.-T. Ding, *Analytical Methods*, 2013, **5**, 5584-5588.

11. Y. Yu, S.S. Naik, Y. Oh, J. Theerthagiri, S.J. Lee, M.Y. Choi, *Journal of Hazard Materials*, 2021, **420**, 126585.

12. N. Idros, D. Chu, *ACS Sensors*, 2018, **3**, 1756-1764.

13. H. Liao, G. Liu, Y. Liu, R. Li, W. Fu, L. Hu, *Chemical Communications*, 2017, **53**, 10160-10163.

14. Y. Zhang, J. Xu, S. Zhou, L. Zhu, X. Lv, J. Zhang, L. Zhang, P. Zhu, J. Yu, *Analytical Chemistry*, 2020, **92**, 3874-3881.

15. Y. Wang, G. Zhao, Q. Zhang, H. Wang, Y. Zhang, W. Cao, N. Zhang, B. Du, Q. Wei, *Sensors and Actuators B: Chemical*, 2019, **288**, 325-331.

16. Y. Niu, G. Luo, H. Xie, Y. Zhuang, X. Wu, G. Li, W. Sun, *Microchimica Acta*, 2019, **186**, 826.

17. J. Pizarro, R. Segura, D. Tapia, F. Navarro, F. Fuenzalida, M. Jesús Aguirre, *Food Chemistry*, 2020, **321**, 126682.

18. M. Yuan, S. Qian, H. Cao, J. Yu, T. Ye, X. Wu, L. Chen, F. Xu, *Food chemistry*, 2022, **382**, 132173.

19. X. Zhang, X. Huang, Y. Xu, X. Wang, Z. Guo, X. Huang, Z. Li, J. Shi, X. Zou, *Biosensors and Bioelectronics*, 2020, **168**, 112544.

20. J. Ma, W. Bai, J. Zheng, *Biosensors and Bioelectronics*, 2022, **197**, 113801.

21. G. Ran, F. Wu, X. Ni, X. Li, X. Li, D. Liu, J. Sun, C. Xie, D. Yao, W. Bai, *Sensors and Actuators B: Chemical*, 2020, **320**, 128326.

22. L. Wang, X. Peng, H. Fu, *Microchemical Journal*, 2022, **174**, 106977.

23. G. Chen, W. Bai, Y. Jin, J. Zheng, *Talanta*, 2021, **232**, 122405.

24. L. Ma, X. Zhang, M. Ikram, M. Ullah, H. Wu, K. Shi, *Chemical Engineering Journal*, 2020, **395**, 125216.

25. T.M. Lima, P.I. Soares, L.A. do Nascimento, D.L. Franco, A.C. Pereira, L.F. Ferreira, *Microchemical journal*, 2021, **168**, 106406.

26. R. Jiang, N. Liu, Y. Su, S. Gao, X. Mamat, T. Wågberg, Y. Li, X. Hu, G. Hu, *Nano*, 2018, **13**, 1850090.

27. M. Baghayeri, H. Alinezhad, M. Fayazi, M. Tarahomi, R. Ghanei-Motlagh, B. Maleki, *Electrochimica Acta*, 2019, **312**, 80-88.

28. L.D. Nguyen, T.C.D. Doan, T.M. Huynh, V.N.P. Nguyen, H.H. Dinh, D.M.T. Dang, C.M. Dang, *Sensors and Actuators B: Chemical*, 2021, **345**, 130443.

29. Y. Li, H. Huang, R. Cui, D. Wang, Z. Yin, D. Wang, L. Zheng, J. Zhang, Y. Zhao, H. Yuan, J. Dong, X. Guo, B. Sun, *Sensors and Actuators B: Chemical*, 2021, **332**, 129519.